Hindawi
Adsorption Science & Technology
Volume 2021, Article ID 6695398, 15 pages
https://doi.org/10.1155/2021/6695398

Research Article

Fabrication of Hybrid Materials Based on Waste Polyethylene/Porous Activated Metakaolinite Nanocomposite as an Efficient Membrane for Heavy Metal Desalination Processes

Mahmoud F. Mubarak[1], **Mohamed A. Zayed**[2], **Ayman Nafady**[3] and **Abeer E. L. Shahawy**[4]

[1]*Applications Department, Egyptian Petroleum Research Institute (EPRI), 1 Ahmed El-Zomer, Nasr City, Box. No., 11727 Cairo, Egypt*
[2]*Chemistry Department, Faculty of Science, Cairo University, 12613 Giza, Egypt*
[3]*Department of Chemistry, College of Science, King Saud University, Riyadh 11451, Saudi Arabia*
[4]*Department of Civil Engineering, Faculty of Engineering, Suez Canal University, Box 41522, Ismailia, Egypt*

Correspondence should be addressed to Mahmoud F. Mubarak; fathy8753@gmail.com
and Abeer E. L. Shahawy; ahmedabeer12000@yahoo.com

Received 18 October 2020; Revised 4 February 2021; Accepted 9 March 2021; Published 20 March 2021

Academic Editor: Adrián Bonilla-Petriciolet

Copyright © 2021 Mahmoud F. Mubarak et al. This is an open access article distributed under the Creative Commons Attribution License, which permits unrestricted use, distribution, and reproduction in any medium, provided the original work is properly cited.

Hybrid nanostructure materials derived from activated metakaolinite are of growing importance due to their intriguing structural/functional properties and promising biomedical/environmental applications, especially designing desalination membranes. Herein, we report procedures to design and fabricate membranes based on waste polyethylene/porous activated-metakaolinite thin film nanocomposites (WPE/PAMK-TFN). It has been devoted to improving water desalination processes, where efficient removal of trace level (~250 ppm) of toxic heavy metals such as Cd(II), Pb(II), and Cu(II) ions from synthetic wastewater solutions was highly accomplished. Physicochemical techniques such as X-ray diffraction (XRD), surface analysis (BET), and Fourier transform infrared spectroscopy (FTIR) have been extensively employed to elucidate the structure/composition of the prepared nanomaterials. The effect of concentration (0–0.5 wt%) of porous activated-metakaolinite (PAMK) on water permeation was investigated. The results obtained revealed that 0.5 wt% of PAMK clay particles produced the highest dispersion, as evident by SEM images of the nanocomposite membranes. Significantly, the constructed membrane showed marked improvements in porosity, hydrophilicity, and hydraulic resistance. Moreover, elemental mapping studies have confirmed the intercalation of activated bentonite clay within the polymer matrix. The obtained results demonstrated that increased flux and rejection capability of membranes occurred at high clay dosage. In contrast, the low rejection capability was observed at either lower pH and higher initial feed concentrations. Ultimately, for 250 ppm of Cd(II), Pb(II), and Cu(II) ions, the constructed membranes showed maximum removal capability of 69.3%, 76.2%, and 82.5% of toxic cations, respectively.

1. Introduction

Over the past few decades, membrane separation was widely accepted as one of the most effective applied techniques in environmental, industrial, and medical applications. Polymeric membranes have become a viable alternative for a wide range of separation processes such as water purification, desalination of seawater, biofuel production, and food fractionation [1]. Reverse osmosis (RO) was considered the most efficient technique for desalinating seawater and recycling wastewater. In this respect, the commonly used traditional thin-film composite (TFC) membranes have a relatively low permeability because of the substantial resistance of the asymmetric polymer support [2, 3]. Thus, the designing of

RO membranes with higher permeate flux, chlorine stability, and more significant, more excellent fouling resistance had been accomplished via exploring new materials and preparation methods [4, 5].

Ali et al. [6, 7] have reported that inorganic exchangeable cations of layered silicates can be substituted with organic cations via ion exchange reactions. In principle, the bonding process between the organic cations and the charged layers of clay is electrostatic. Simultaneously, Van der Waals induces attraction forces between the organic species and the silicate surface. Due to the discharge of large amounts of contaminated industrial wastewater, they are bearing pollutants such as Cd, Cr, Cu, Ni, Pb, Zn, and As are the most hazardous chemical-intensive industries [8, 9]. Therefore, it is necessary to treat metal-contaminated wastewater before its discharge into the environment. Conventional treatment methods such as chemical precipitation, ion exchange, and electrochemical removal can achieve heavy metal removal from the inorganic effluent. However, these methods have drawbacks, including incomplete elimination, high-energy consumption, and toxic sludge production [10, 11].

Clay minerals are members of the phyllosilicate or sheet silicates family, consisting of hydrated alumina–silicates. Phyllosilicates are a crucial essential group of minerals that include micas, chlorite, serpentine, talc, and clay minerals. The basic building blocks of clay minerals are tetrahedral silicates and octahedral hydroxide sheets. The arrangement of tetrahedral and octahedral sheets gives rise to various minerals classes such as 1 : 1 and 2 : 1. The 1 : 1 clay consists of one tetrahedral and one octahedral sheet (e.g., kaolinite that has been exploited for their potential biomedical applications), whereas the 2 : 1 clay consists of an octahedral sheet sandwiched between two tetrahedral sheets (e.g., smectite, chlorite, and vermiculite).

Regarding kaolin, when the 1 : 1 sheet occurs in stacks, the OH ions of one sheet lie next to and in close contact with the O_2-layer of its neighbor. Because of this arrangement, the positive charge of the H^+ ions in the OH^- layer exerts a strong attraction for the neighboring sheets' harmful oxygen. In this way, the platelets of kaolinite are tightly bound together. Kaolinite is a nonexpanding mineral; hence, it is unable to absorb water into the interlayer position. Kaolinite has a basal spacing fixed at 0.72 nm, which is small compared to the other clay minerals. Previous work has shown that kaolin is not highly stable in alkaline media, and different zeolitic materials can form. For this reason, kaolin is usually used after calcination to obtain the more reactive metakaolin phase. After endothermic dehydroxylation, kaolin is transformed into amorphous metakaolin [12].

Clay composite membranes have been utilized in various applications, including evaporation, greywater purification, sodium dodecylsulphonate separation (SDS), and membrane distillation [13, 14]. Recently, Prince et al. [15] have investigated hydrophobic preparation using waste polyethylene-(WPE-) clay nanocomposite nanofiber membranes for desalination processes with a rejection flow rate above 80% and 20 L/hm^2, respectively. However, to the best of our knowledge, the use of functionalized porous activated metakaolinite composite thin film (PAMK-TFN) membranes for the desalination of heavy metals is undeveloped. Thus, the present work has focused on investigating the fabrication and application of the waste polyethylene/polyamide-metakaolin thin film nanocomposite(WPE/PAMK-TFN) membranes for the removal of toxic heavy metals from synthetic wastewater solutions, in particular Cu(II), Pb(II), and Cd(II). One of this research's key features is that the thin film has been created using an internal coating process [16]. Additionally, critical operating conditions such as pH, contaminants, and concentrations of ions, along with permeate flux, had been carefully probed to optimize the experimental parameters that enable efficient removal of these heavy metals.

2. Experimental

2.1. Materials. The polysulfone (PSF) (MWCO = 8000) ultrafiltration hollow fiber membranes had been used as substrates. The natural kaolin was collected from the area of Kutch, Egypt. The natural well-crystallized kaolin (a mixed source for silica and alumina) had been obtained from the kaolin deposits in southern Sinai. Metakaolinite was obtained via calcination of kaolin at 650°C for 2 h in a muffle furnace. Film grade high-density polyethylene (HDPE) and linear low-density polyethylene (LLDPE) were purchased from Reliance Industries, Egypt. The other chemicals, including polyvinyl chloride, H_2SO_4 (98%), and ethyl alcohol (absolute 99.9% = GR), were purchased from Sigma-Aldrich and used as received for interfacial polymerization.

2.2. Synthesis of Waste Polyethylene/Porous Activated Metakaolinite Nanocomposite Membrane. Asymmetric polymeric layers of waste polyethylene (WPE) membrane (HDPE and LLDPE) with activated metakaolinite nanoparticles were synthesized using phase inversion induced by immersion precipitation. First, both PE (HDPE/LLDPE mixture) and xylene (500 ml) were gradually added into the reactor under stirring pressure. In case that PE started to melt in the homogeneous dough forming reactor, 4 L of toluene was then added gradually, by which the reactor temperature became 95°C.

The activated metakaolinite-embedded layers were prepared by dissolving 0.1 g of metakaolinitein 90 mL of xylene solvents for 3 h by mechanical stirrer at 400 rpm and room temperature [17]. The above mixture was added to the 500 ml solution of polymer and then stirred for 6 h at 800 rpm and 45°C. After forming a homogenous solution, the films were cast of 250 μm thickness with a filmography (K4340 Automatic Film Applicator, Elcometer) in an atmosphere with controlled relative humidity polysulfone as a support layer and that evaluated using SEM analysis. The polymer solution had been intruded into support layer pores before casting. For precipitation, the prepared films were immersed in a nonsolvent bath (35° C distilled water) [18]. Afterward, the membrane was regularly cleaned with clean water to extract the residual solvent and store it wet. Eight similar membrane sheets were made and tested for each composition of the polymer solution to achieve an average value of flux and retention of the solute.

2.3. Physical Methods for Characterization of Nanocomposite Membrane. To prevent charge accumulation, thin sections of the activated metakaolinite composite membranes mounted on specimen gold-coated and 3 kV images investigated using scanning Electron Microscope (SEM). Nanofibers' surface patterns were analyzed using an atomic force microscope (AFM, Bruker Multimode 8HR) in tapping mode. Equilibrium contact angles within 5 s of placement of each drop were calculated at different membrane locations. Analysis of X-ray diffraction (XRD) was performed using XRD-X'Pert PRO diffractometer (P-Analytical, The Netherlands) using copper Kα ($\pi = 0.1542$ nm at 35 kV and 35 mA) as the radiation source. The diffractogram was scanned in a 2θ range of 1.5–10 with a scanning rate of 2° min^{-1}. The d spacing of the C15A in composite was calculated using Bragg's equation (1)based on XRD results:

$$d = \frac{n\lambda}{2\sin\theta}, \tag{1}$$

where d is the spacing between layers in the clay structure, λ is the wavelength of X-ray equal to 0.154056 nm, θ is the angle at the maximum point of the first peak (lowest θ) in the spectra, and n is an integer, representing the order of diffraction where $n = 1$ in our calculation. FTIR spectra of the activated metakaolinite composite membranes were recorded in the wavenumber range of 4000–400 cm^{-1} using ATR-FTIR spectroscopy (Agilent Technologies, Cary 660). A ffTA Foram X3 multiwavelength Raman spectrometer was used to acquire Raman scattering spectra over a range of 200–2200 cm^{-1}, with a resolution of 4 cm^{-1}, using a backscattering configuration using a 20× objective excited with a 532 nm laser diode [19].

Pore size measurements were performed using a Porosimeter II produced by Beckman Coulter (UK). Porosity was calculated from the weight and volume of a disk and the polymer's actual density used to manufacture it. The surface area and pore size analyzer Nova 1000e (Quantachrome, UK) was used to measure the specific surface area of the modified polyethylene membranes using nitrogen adsorption according to the Brunauer–Emmett–Teller (BET) method. Before gas adsorption, small samples (300 mg) of the Vyon material were degassed and dried in a vacuum at 100°C for 2 h.

2.4. Porosity and Membrane Pore Size Measurements. The overall membrane porosity (%), ε, which is defined as the volume of the pores per the total volume of the porous membrane, was calculated using the following equation:

$$\varepsilon(\%) = \frac{\left(W_{\text{wet}} - W_{\text{dry}}\right)/\rho_w}{\left(\left(W_{\text{wet}} - W_{\text{dry}}\right)/\rho_w\right) + \left(W_{\text{dry}}/\rho_w\right)}, \tag{2}$$

where ε is the membrane porosity (%),w_{wet} is the weight of wet membrane (g), w_{dry} is the weight of dry membrane (g), ρ_p is the density of the polymer (g cm^{-3}), and ρ_w is the density of water (g cm^{-3}).

To calculate the distribution of the membrane bubble point and a pore size distribution, a PMI capillary flow porometer (Porous Materials Inc., USA) was employed. A sample chamber has placed a bundle of hollow fibers thoroughly wetted with isopropanol (surface tension = 21.7 dynes per cm) and sealed. Pure nitrogen was then slowly delivered into the chamber until the pressure reached a point, overcoming the cap. This point reflects a bubble point in the membrane. The diameter of the pores can then be determined using the following equation [20].

$$d_p = \frac{4\gamma\cos\phi}{P}. \tag{3}$$

The pore size diameter, γ is the surface tension of the liquid, ϕ is the contact angle of liquid, and P is the external pressure.

2.5. Chemical Analysis. A photometer (HACH LANGE, LASA 100) with cuvette was used in measuring the concentrations of Cu(II), Pb(II), and Cd(II) ions in feed, permeate, and retentate solutions.

2.6. Membrane Performance Test

2.6.1. Experimental Work for Filtration Efficiency. A cross-flow stainless steel nanofiltration unit was employed to study the membrane permeability, flux, fouling, and rejection shown in Figure 1. This system has one membrane module with an effective membrane area of 0.00076 m^2, which can be operated at a pressure range of 1 to 5 bar. The nanofiltration unit consisted of a feed tank (capacity 5 L), a membrane assembly, a high-pressure pump (Tuthill Pump Co., from California), and two pressure gauges. At the inlet and outlet membrane module, there were two flow meters for measuring feed and retentate flow levels (MPB Industries, Kent, England). In this job, the flow rates were kept at 0.4 L/min for feed and retentate. Three control valves (Ham-Let, UK; H6800 for valve 1, H300SSLR1/4RS for both valve 2 and valve 3) controlled the fluid flow at locations (Figure 1).

A prepared membrane was applied to test membrane filtration at room temperature ranging from 22 to 25° C. The prepared membrane is a polyamide membrane of a very thin active semiaromatic polyamide layer centered on piperazine with a supporting layer of microporous polysulfone [10, 12]. The prepared membrane is of pore size distribution obtained using a solute transport system. The membrane surface roughness was investigated using AFM and presented in a previous paper [13]. Several researchers have been previously devoted to the surface charge at various pH and the isoelectric point of the prepared membrane [21]. The membrane's surface is charged positively if the solution pH is less than 3.3–4 and negatively charged if the solution pH is greater. This phenomenon occurs in thin-film composite membranes from the dissociation of various functional groups (typically carboxyl) located on the membrane surface with the pH and amino pendants. The membrane was immersed in deionized water, and each membrane was pressurized for at least 2 hours at 5 bars. Pure water was used during measurements to avoid any compression effects and assess the leaks' tightness.

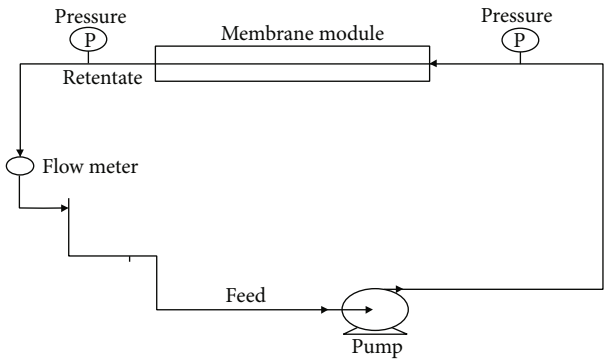

Figure 1: Schematic diagram of cross-flow WPE/PAMK-TFN membranes filtration unit.

2.6.2. Permeability of the Prepared Membranes. Measurements of water flux were performed with high purity Milli-Q water (resistivity 18.2 MΩ cm). The pure permeability of water was determined from filtration tests at various transmembrane pressures (1.5–5 bar) at ambient temperature with a membrane area of 0.00076m^2. The pressure was ranged from 1.5 to 5 bar maximum pressure. Using the pump's focus outlet valve and variable speed switch, the transmembrane pressure and volumetric flow rate were modified at some pressure. Pure water flux can be described as:

$$J_V = Q.A, \tag{4}$$

where $J_{v=}$permeate flux(L/m^{2}h), A = effective membrane area(m^2), and$Q$ = Volume flow rate(L/h).

Nonetheless, in this study, the pure water flux was determined using an electronic balance to measure the obtained permeate over a predetermined time (Precisa, Model XB3200C) connected to a computer. By plotting the membrane flux (J_v) for a variety of applied pressure (ΔP), the membrane permeability (pure water permeability), L_p can be obtained from the slope of the straight line as follows:

$$L_P = J_V.\Delta P. \tag{5}$$

2.6.3. Heavy Metal Retention Using WPE/PAMK-TFN Membranes. An initial volume (~500 mL) of the metal ions Cu(II), Pb(II), and Cd(II) solution was pumped and circulated via the membrane module (Figure 1). Permeate was continuously collected in a beaker until 50 g of permeate was obtained, and the experiment was paused. The permeate flux was measured during the experiment by measuring the obtained permeate, as set out in Section 2.3. Final permeate flux (i.e., when the mass of permeate = 50 g) was used to describe the findings unless otherwise mentioned. Table 1 summarizes the experimental conditions used to test the effect of metal solutions on pressure, metal concentration (carbon), and pH (adjusted using 1 M NaOH or 1 M HNO_3). A fresh piece of the NF270 membrane was used in each experiment. Solute separation or removal can be interpreted by a factor of refusal (R):(3) $R = 1 - C_pC_b$, where C_p is the concentration of solute in permeate, and C_b is an average bulk concentration of solute in the feed (C_f) and concentrates/retentate (C_r).

Table 1: Membrane experimental conditions.

Exp.	C_{metal} (mg/L)	pH_{metal}	Pressure (bar)
1	100, 250, and 500	2-11	10-50

$$C_b = \frac{C_f + C_r}{2}. \tag{6}$$

2.6.4. Studying of the Adsorption/Deposition of Membrane Solute. Solute adsorption tests on the NF270 membrane were performed inside a closed bottle by measuring the metal concentration with the membrane before and after 24 hours of contact time. The bottles were shaken at regular intervals during the experiments to avoid settling. Metal solution volume and initial concentrations were 500 mL and 1000 mg/L; considering the molecular weight of tested metals, the initial concentrations (1000 mg/L) of cadmium, copper, and lead were 8.90, 15.74, and 4.82 mmol/L, respectively. The total region of surface (A) of the membrane was 25 cm^2. A blank experiment determined the effect of water evaporation and the solute's adsorption on the recipient walls. The adsorption amount Q (mg/m^2) was determined using [21, 22]:

$$Q = \frac{\left[\left(C_i - C_{eq}\right) - \left(C_i - C_{blank}\right)\right] \times V}{A}. \tag{7}$$

C_i, C_{blank}, and C_{eq} are the initial, blank, and equilibrium concentrations in mg/L or mol/L.

2.6.5. Adsorption Experiments. The adsorption solution of heavy metal ions was prepared into 500 mL deionized water. For adsorption experiments, 10 mg of the membrane was soaked in 15 mL heavy metal ions solution with 100 rpm shaking speed at 25°C. The pH values were controlled by 0.1 mol/L H_2SO_4 or 0.1 mol/L NaOH solutions. The adsorption process lasted for 24 h with original heavy metal ions concentration of 500 mg/L at room temperature. The adsorption isotherms of heavy metal ions were constructed via initial concentrations in the range of 10-250 mg/L. The adsorption amount q (mg/g) of heavy metal ions for WPE/-PAMK-TFN membrane was determined based on the equation (1):

$$\frac{(C_0 - C_e)V}{m} \tag{8}$$

C_0 and C_e (mg/L) were the original and balanced concentrations of heavy metal ions in the solution. V (L) was the solution's volume, and m (g) was the initial membrane's weight.

3. Results and Discussion

3.1. Membrane Morphology and Chemical Composition. SEM images (Figure 2) show the morphology of metakaolin and

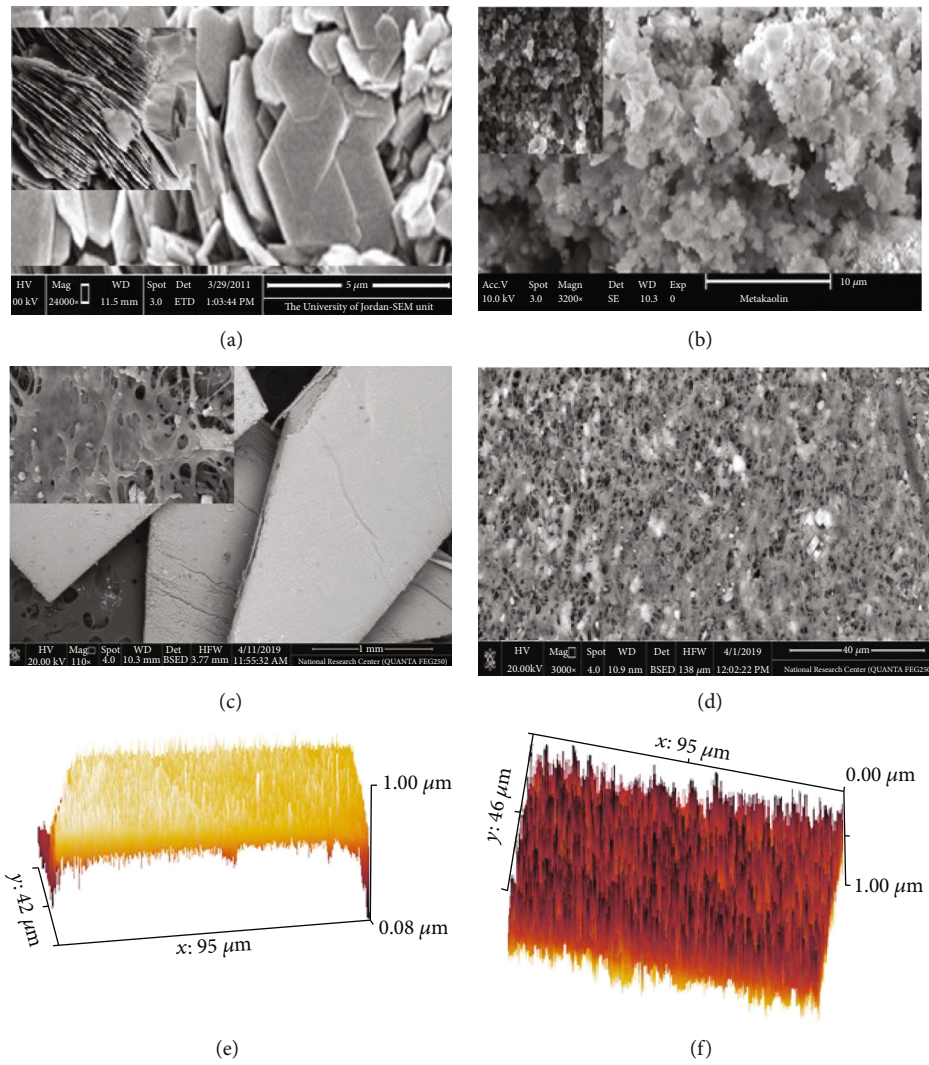

Figure 2: FESEM images of the (a) kaolin, (b) metakaolinite, (c) polyethylene membrane, (d) WPE/PAMK-TFN membranes, AFM of (e)polyethylene membrane, and (f) WPE/PAMK-TFN membranes.

WPE/PAMK-TFN membranes, revealing a noticeable shift in the starting materials' initial surface morphology. Kaolinite has a platy morphology and hexagonal outlines (Figures 2(a) and 2(b)).WPE/PAMK-TFN membranes with a macro-void-free cross-sectional structure are favored in NF because they can have (1) a high mechanical strength to maintain high operating pressure, (2) a less defective surface for high rejection, and (3) a more uniform distribution of pore size [23]. The ways to WPE/PAMK-TFN membranes have been summarized in literature [24]. A WPE/PAMK-TFN membrane was therefore achieved in this study by dope conditions solution. The FESEM images of WPE and WPE/-PAMK-TFN membranes are shown in (Figures 2(c) and 2(d)). At a lower magnification (Figure 2), the cross-section of the membrane appears relatively small. However, a highly porous structure can be observed (Figures 2(c) and 2(d)). No clear regular pore structures can be seen on the exterior surface (Figure 2(c)) [17], suggesting that the selective membrane layer is a defect. The substrate's inner layer can also pose little resistance to water transport, as wide holes can be found on the inner surface (Figure 2). Few tiny nodules are observed on the membrane surface after cross-linking WPE/PAMK-TFN (Figures 2(c) and 2(d)). Upon adsorption of heavy metals, the membrane becomes of a little roughness (Figure 2(d)) [25].

AFM images of the surface properties of the WPE membrane and WPE/PAMK-TFN are shown in Figures 2(e) and 2(f); it shows the topology of the WPE membrane. Figure 2(f) shows WPE/PAMK-TFN for a fixed polymer content of 20 wt.%.

The roughness of the WPE membrane increased with the increase of metakaolin concentration. This addition probably formed very tight nodules creating a rough surface indicated by high roughness parameter values [26]. It is possible to detect the presence of notable peaks on the surface of the doped layer surface due to the introduction of metakaolin nanoparticles into the polymer solution; therefore, some remain on the surface of the material. Figure 2(f); demonstrates an additional surface roughness analysis considering the mean roughness parameter values for the manufactured

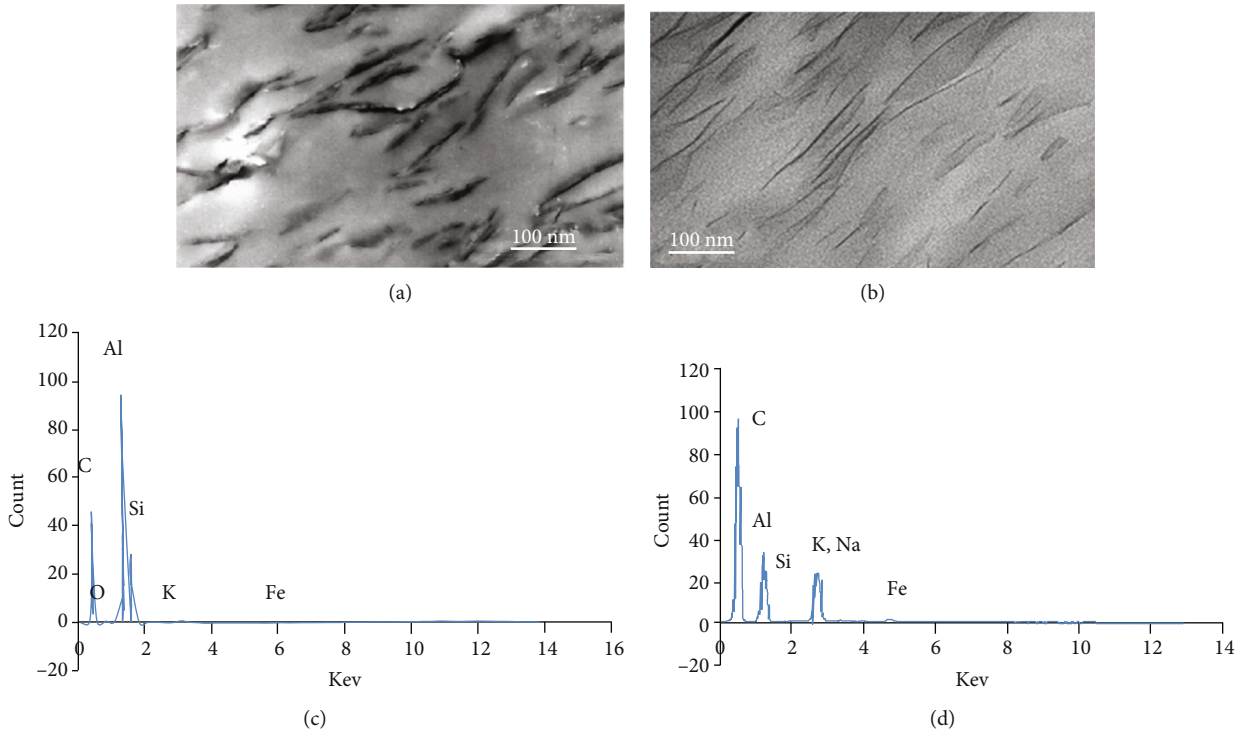

Figure 3: HR-TEM ((a) and (B)) and EDX ((c) and (d)) of WPE/kaolin and WPE/PAMK-TFN membranes.

sheet. Figure 2(f) displays the presence of metakaolin in the layer contributes to a growing increase in surface roughness. This fact may be related to an increase in pore size and porosity of the WPE layer surface. This trend is coherent with the SEM and TEM images shown in Figures 2(c) and 2(d). An increase in metakaolin content on the WPE membrane surface and the size of metakaolin clusters were produced due to nanoparticle agglomeration results in increased surface roughness of metakaolin-doped materials (Figure 2(f)) [27].

3.2. TEM and Elemental Mapping. A general view of the metakaolin micrographs in pristine WPE membrane, bleached, and functionalized metakaolin can be observed in Figures 3(a) and 3(b).

The more robust particle's intermolecular forces, namely, cohesive tension, can lead the metakaolin particles to aggregate and form the agglomerates. It can be seen from Figure 3(a) that the kaolinite mineral possesses pseudohexagonal plate-like particles with widely irregular shapes, rough surfaces, and different particle sizes (smaller than 120.5 nm). The TEM images of the metakaolin composites are presented in Figure 3(b), and the mapping of C, N, O, Si, Al, Fe, and Ca elements is measured by EDx. These figures show good dispersion distributions of the metakaolin particles more than kaolin in the WPE membrane, with some aggregates in both the kaolin and metakaolin composites membrane. Furthermore, EDx analysis proved the presence of metakaolin particles on the surfaces based on the elemental analysis data of alumina and silica oxides in significant quantities, with traces of other minerals such as iron and calcium minerals absent in the case of metakaolin. Figure 3(b) shows the morphological evolution due to intercalation metakaolin by DMSO and MeOH molecules. The modification of kaolinite powder by MeOH molecules during the synthesis process leads to the destruction of the metakaolin's kaolinite nature's hexagonal structure to be smaller particles, resulting in a fair distribution of metakaolin particles in the polymer matrix [26]. Figure 3(b) presents TEM images of the composites based on metakaolin particles. The micrographs show excellent dispersion–distributions with no agglomeration; indeed, the functionalized metakaolin exhibits average sizes of approximately 101 nm. These results indicate that exfoliation of metakaolin layers has occurred in the nanocomposites. Figures 3(c) and 3(d) represent EDx images of WPE/kaolin and WPE/PAMK-TFN membranes and their corresponding spectra of 6 peaks.

The significant elements detected in WPE/kaolin and WPE/PAMK-TFN membranes are silicon and aluminum and little potassium, as demonstrated in Figures 3(c) and 3(d). The EDX peaks of the membrane samples indicated that kaolin contains five elements, namely, C, H, Al, Si, and K. The EDX analysis result shows dealumination, of kaolin to produce metakaolin that is used in the membrane for application in heavy metals removal shows silicon content increases and the aluminum content decreases that confirm the presence of metakaolin constituent in the membrane.

The physicochemical properties of the composite membrane WPE/PAMK-TFN were analyzed using FTIR and XRD to examine changes in functional groups and phase transition posed in the membrane WPE/PAMK-TFN. FTIR is given in Figure 4.

As sketched out in Figure 4, characteristic bands at 3687 and 3618 cm^{-1} were found, assigned to the OH stretching vibration structural [27]. In contrast, the absorption bands

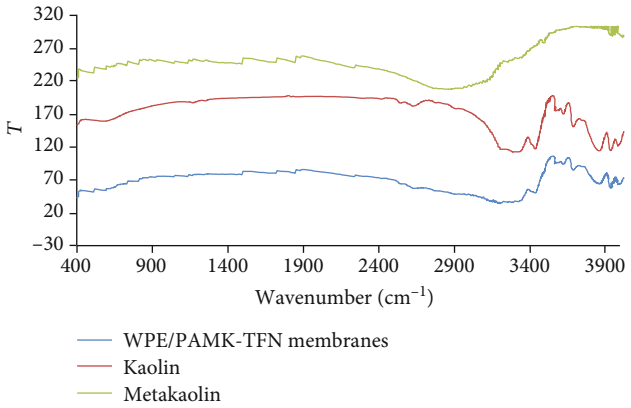

Figure 4: FTIR spectra of kaolin, metakaolin, and WPE/PAMK-TFN membranes.

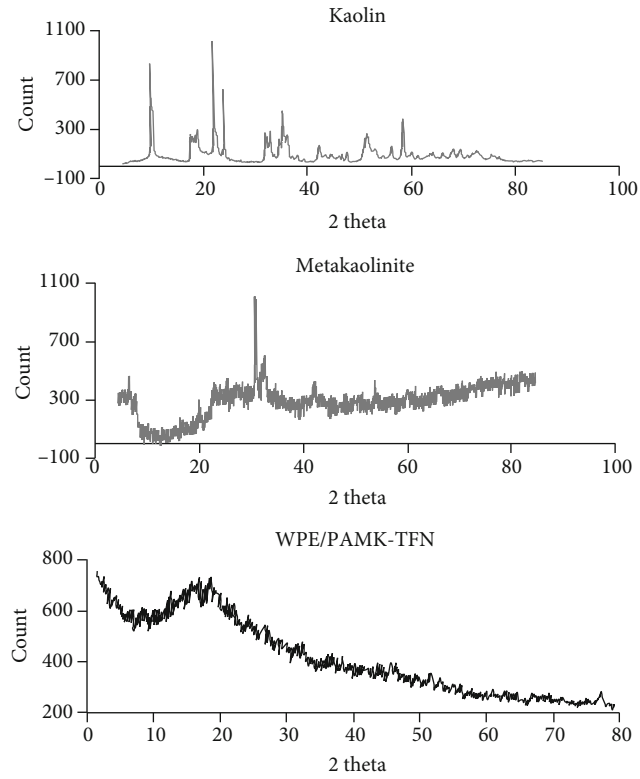

Figure 5: The results of XRD analysis of kaolin, metakaolin, and WPE/PAMK-TFN membranes.

were due to the structural OH bending vibration for the metakaolinite precursor at 1578 and 1486 cm^{-1}. The octahedral layer of the metakaolinite structure, where aluminum atoms were octahedrally coordinated to hydroxyl groups and shared apical oxygen from the tetrahedral silica surface, exhibited these OH stretching and bending vibrations. Because of the sintering process, all WPE/PAMK-TFN membrane spectra diminished these characteristic bands for kaolinite structure completely. These findings suggested the complete dehydroxylation of metakaolinite in which the metakaolinite structure di-octahedral 1 : 1 layer was collapsed due to the removal of water during the sintering process. The average (unheated) kaolin and metakaolin XRD patterns are shown in Figure 5.

The starting content includes 72 wt. percent of kaolin, 27 wt. according to XRD results, percentage of quartz, and a small quantity (about 1 wt. percent) of other components. As stated in previous studies, kaolinite is described by its characteristic X-ray diffraction peaks at 12.34 and 24.64 2 h. Save for the peaks due to admixed impurities, the XRD pattern of metakaolin obtained by heating the kaolin for 3 h at 650 C resembled others. The XRD patterns show a significant shift after thermal treatment compared to the untreated kaolin pattern, distinguished by the absence of kaolin diffraction peaks, followed by the emergence of amorphous aluminosilicates. Metakaolin has an amorphous structure, and the highest diffraction peaks correspond to the very typical presence of quartz (SiO_2) (Figure 5). The only crystalline phase in metakaolin [28] is quartz.

The XRD studies showed that SiO_2 was also present in the membrane, in addition to the WPE/PAMK-TFN membranes. Consequently, the scaling was possibly the primary explanation for the observed decrease in module efficiency during the first 5–6 h of MD process activity, as indicated in previous studies; kaolinite is defined in 12.34 and 24.64 2 h with its characteristic X-diffraction peaks. Apart from the peaks due to mixed impurities, the XRD pattern of metakaolinite is obtained by heating the kaolin for 3 h at 650°C resembled others. The XRD patterns indicate a significant change after thermal treatment compared to the untreated kaolin sequence, distinguished by the disappearance of the kaolin diffraction peaks, accompanied by the emergence of amorphous aluminosilicates [29]. Metakaolinite is of amorphous form, and the highest diffraction peaks correspond to the very regular presence of quartz (SiO_2) (Figure 5). In metakaolinite, the only crystalline form is quartz [30].

Porosimetry was used to calculate a pore size distribution for a given porous structure. The recorded parameters included maximum, minimum, and mean pore sizes. It was found that porosimetry measurements for polyethylene and NF WPE/PAMK-TFN membranes within the experimental error were very similar (Table 2).

It suggested that treatments result in a noticeable reduction of the membrane's porosity characteristics; therefore, the functions of the modified membranes were impaired by the addition of metakaolin, and requirements of the accessibility of the composite NF WPE/PAMK-TFN membranes were successfully achieved [31].

Since only milligrams of metakaolin were added during the membrane casting, it was possible to assume that if the metakaolin was spread evenly throughout the pore structure and that it is not surprising that this quantity of metakaolin would be closing the pore structure to a point where this technique would measure it. Surface area analysis was carried out to determine if the metakaolin changed the membranes' total surface area [32]. Unfortunately, it was impossible to get reliable results due to the low surface area of the HDPE membranes, which was lower than 1–5m^2g^{-1}—a minimum surface area required for reliable BET measurement using nitrogen porosimetry.

Table 2: Porosimetry data for polyethylene and NF WPE/PAMK-TFN membranes.

Treatments	Minimum pore, nm	Maximum pore size, nm	Mean pore size, nm	Surface area, m^2/g
Polyethylene	500	1000	750	120
NF WPE/PAMK-TFN membrane	50	100	40	560

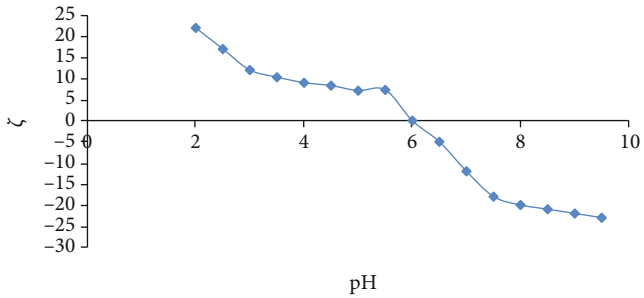

Figure 6: Zeta potential (ζ) of WPE/PAMK-TFN membrane against pH using 1 mMKCl solution.

3.2.1. Surface Charge Properties of NF WPE/PAMK-TFN Membrane. The experimental results for calculating the WPE/PAMK-TFN membrane surface zeta potential in the 3.0 to 9.5 pH range using 2 mM KCl electrolyte are shown in Figure 6.

Membrane charge is a function of many processes, where the most important ones are the adsorption of various charged electrolyte solutes and the detachment of functional membrane groups. The zeta potential (UP), as seen, varies with the pH [22]. The membrane is charged positively at pH 3.0. The membrane surface zeta potential decreases at the higher pH values until the isoelectric point (pH 6.2) and is charged negatively above this value. The membrane's net charge around the isoelectric point is nearly zero, where the membrane functions as a nonpolar sheet [33].

3.3. Membrane Adsorption Isotherm. Adsorption isotherms reflected the variation of adsorption amount at various adsorbate concentrations. The Freundlich and Langmuir isotherm models were applied to sketch the equilibrium process of heavy metal ions adsorption onto the WPE/PAMK-TFN membrane. The isotherm equations were expressed as follows [11]:

$$\frac{C_e}{q_e} = \frac{1}{q_m K_L} + \frac{C_e}{q_m}, \tag{9}$$

$$\log q_e = \frac{1}{n} \log C_e + \log K_F, \tag{10}$$

where q_e (mg/g) was the maximum adsorption amount, and K_L was the Langmuir isotherm constant in the free energy and the binding strength. K_F and n were Freundlich constants involved in the adsorption amount and the intensity of adsorption, respectively.

The suited lines for the isotherm adsorption model were exhibited in Figures 7(a) and 7(b), respectively.

The relevant isotherm adsorption dates were concluded in Table 3. By comparing R^2 values of WPE/PAMK-TFN membrane, the Langmuir model ($R^2 < 0.99$) was not suitable for equilibrium data than Freundlich model (0.989, 0.9985, and 0.999), suggesting the heavy metal ions adsorption showed the multilayers coverage on the adsorbent surface; which indicates that the multilayer adsorption behavior also acted a significant part during the adsorption process. The maximum heavy metal ions adsorption amount for WPE/-PAMK-TFN membrane was superior to most reported heavy metal ions adsorbents in the literature, as illustrated in Table 4.

3.4. The Mechanical Property of the Filtering Membrane

3.4.1. Membrane Performance Evaluation

(1) Effect of Feed Solution Concentration. A series of saline solution concentrations (200-1000 mg/L NaCl) was tested as a critical operating parameter to investigate further the relationship between ion concentration and the electrostatic repulsion force's effectiveness. In the WPS, WPS/kaolin, and WPE/PAMK-TFN membranes studies of various types of saline water presented, the obtained degree of heavy metals rejection reached 100, 60, and 40%, with a maximum flux range from 0.05, 0.2, and 0.35 $m^3/h/m^2$ for WPE/PAMK-TFN WPS, WPS/kaolin membranes, respectively. Hence, the concentration of heavy metals ions in the feed was below 1 mg/L, as shown in Figure 8 for WPE/PAMK-TFN membrane, and that acceptable for membrane desalination more than the other two membranes. A gradual decrease in the draw concentration and osmotic driven force resulted in increased water flux for WPE/PAMK-TFN WPS, WPS/kaolin, and WPE/PAMK-TFN membranes, as displayed in Figure 9.

However, due to a high heavy metals ions concentration in tested bilge water, it should be expected that OH scales might form a scaling layer on the membrane surface during feeding concentration [39]. Further research on this phenomenon in the WPS/kaolin and WPE/PAMK-TFN membrane tests, a continuous concentration of feed was performed further to achieve a water recovery above 80 and 25 percent at the beginning of the WPE/PAMK-TFN and WPS/kaolin membranes assembly. Concerning WPE/-PAMK-TFN membrane, high salinity solution was used to rinse the permeate flux from 0.01 to 0.05 $m^3/h/m^2$.

It can be said that for WPE/PAMK-TFN and WPS/kaolin membranes at low initial metal ion concentration, the ratio of the metal ions to the available adsorption sites is low. Consequently, the adsorption is independent of the adsorbents. However, as the number of M^{2+} increases, the adsorbent's

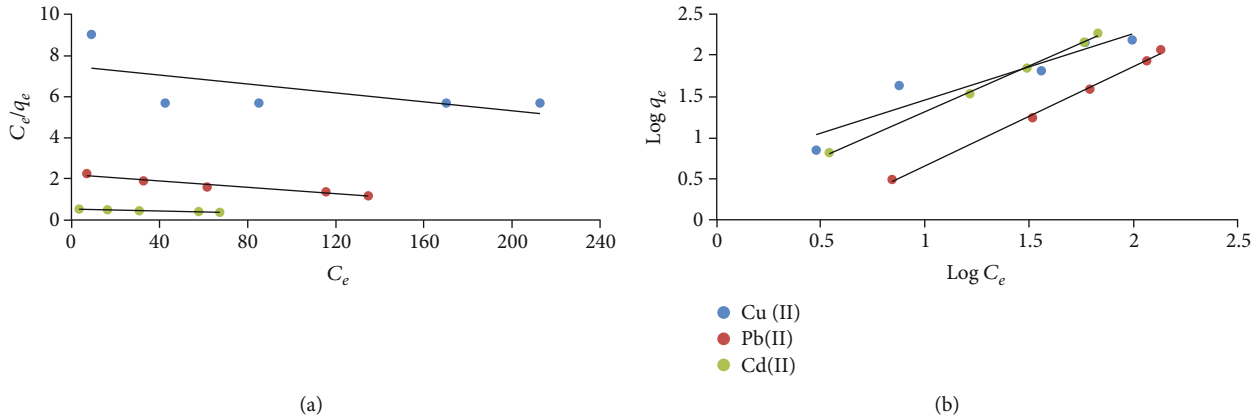

Figure 7: Adsorption isotherm of heavy metal ions on the prepared WPE/PAMK-TFN nanocomposite membrane (a) linear Langmuir and (b) linear Freundlich.

Table 3: Adsorption isotherm parameters of heavy metal ions on the prepared WPE/PAMK-TFN nanocomposite membrane.

Isotherm model	Heavy metal ions		
	Cu(II)	Pb(II)	Cd(II)
Langmuir isotherm linear regression			
K_L (lm/g)	0.001447	0.0035882	0.0042582
Q_{max} (mg/g)	50.25	22.8	22.3
R^2	0.6192	0.9775	0.9877

Table 4: Comparison of adsorption capacity of WPE/PAMK-TFN nanocomposite membrane with other reported adsorbents.

Adsorbent	q_m (mg/g)	Experimental conditions	Ref.
PS fibrous with CS-rectorite nanospheres	134.0	0.1 g samples into the flask with 150 mL Cu^{2+}, the temperature at 25°C, agitation speed 100 rpm, pH 5.0, (PS/CS) and(PS/CS-REC) owned the maximum removal rate about 73% and 93%, respectively, time 90 min	[34]
CS/PEO/activated carbon nanofibers	195.3	50 mg of CPANM in 20 mL of specified metal ion solution, 50 mg initial dosage, 50 mg/L initial conc., 25°C room temperature, maximum removal (%) was noticed at pH value 3, 3, 5, 5, and 5 for Cr(VI), Fe(III), Cu(II), Zn(II), and Pb(II) ion, respectively. For all five metal ions, more than 80%. Within 11 min	[35]
CS/PVA nanofibers	90.3	The adsorption of Cu(II) onto the positively charged PVA/CS nanofiber membrane (pH < 6) Cu(II) by the PVA/CS nanofiber was established within 120 min, adsorbent dosage 0.5 g/l, the temperature of 20 ± 10 C	[36]
CS beads	80.7	A pH of 6.0, the contact time of 90 min, with constant chitosan and cross-linked chitosan beads weight (0.010 g), solution volume 100 ml, agitation speed500 rpm, Cu(II) concentration of 5 ppm	[37]
Amine grafted CS nanofibers	166.7	Equilibrium time (8 h) and 25°C	[38]
CS-L3 membranes	276.2	At pH 7, the metal removal percent efficiency values were estimated and found to be 91.6% and 84.6%for initial metal ion concentration of 550 mg/L of Pb(II) and Cd(II) ions, respectively	This study

unit mass exposes to more metal ions, and the adsorbents with more available binding sites would take up more metals.

Copper, lead, and cadmium removal are seen in Figure 10 at various feed concentrations (100–1000 mg/L). At low concentration, the rejection was higher for cadmium, copper, and lead, and as the concentration of the metal solution increased, the rejection decreased. WPS/kaolin and WPE/-PAMK-TFN membrane can altogether remove Cu at 100 and 500 mg/L and a concentration of only 46 percent at 10 bar at 1000 mg/L. However, the rejections at a higher concentration of 10,000 mg/L have a higher standard deviation of 14 and 20, respectively. For lead and cadmium ions, the 100 mg/L rejection was 93 ± 5.2 percent, and 99 ± 4.5 percent, 20 percent, and 94 percent, respectively, were rejected

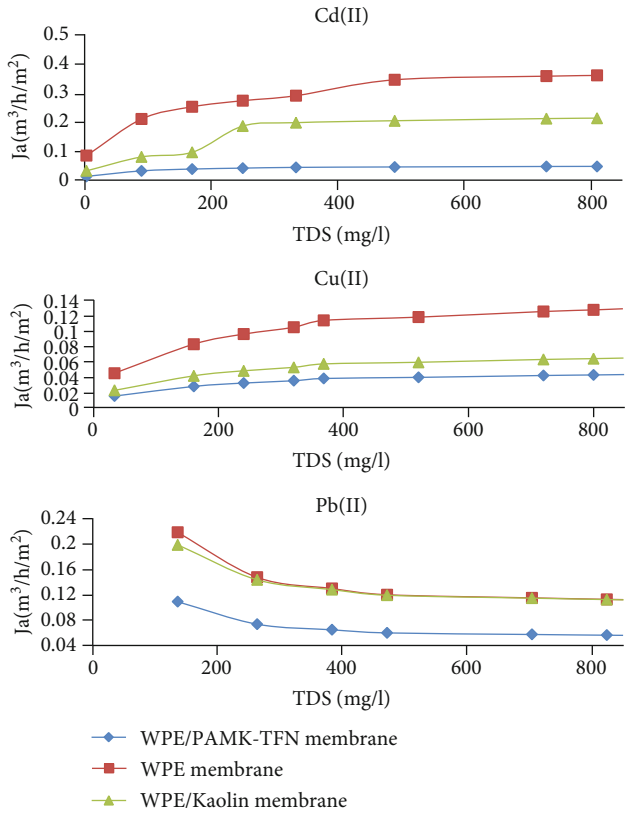

Figure 8: Effect of heavy metal feed concentration on WPS, WPS/kaolin, and WPE/PAMK-TFN membrane flow rate.

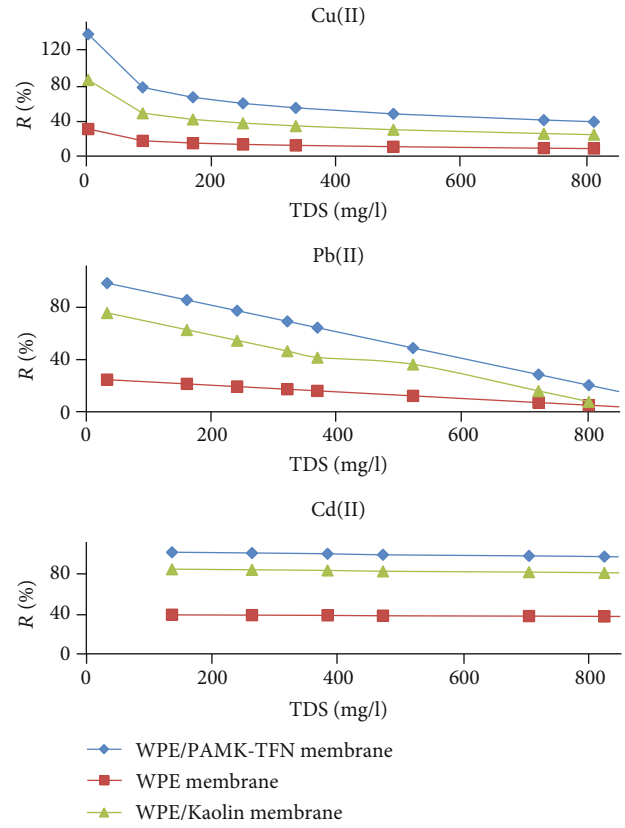

Figure 9: Effect of heavy metal feed concentration on WPS, WPS/kaolin, and WPE/PAMK-TFN membrane rejection.

at 10,000 mg/L. The pattern of decreasing refuse as the concentration of metals increased was also stated in the literature for the same WPS/kaolin and WPE/PAMK membrane.

(2) Effect of Pressure. Polarization of the concentration, which increased with increasing strain, contributes to decreased retention. Convective transport, however, allows retention to increase. The counteracting contributions of increased convective transport and increased polarization of concentrations contribute to an almost constant retention value [40]. Figure 10 shows all used metals influence, but with some differences, on both concentration polarization and convective transport.

For example, copper rejection at pressure = 20 bars was 90% and then decreased at higher pressures; in other words, concentration polarization was accompanied by convective transport and concentration polarization. When the pressure applied grew, Pb(II)'s dismissal rose marginally (20% to 98%). Cadmium and lead acted differently: the rejection improved when the pressure improved from 20 bar to 100 bar, but the rejection decreased in Cd(II) when the pressure rose to 40. Rejection increased or decreased marginally, with increased pressure. The minor variations between the release of Cu, Cd, and Pb since the increased pressure may be attributable to a higher water permeation at higher pressure or at a solute diffusion rate not anticipated to be substantially influenced by higher pressure since the solution concentration is mainly controlled [41]. Cd, Cu, and Pb averaged 90, 92, and 80 rejections, respectively. The explanation for the more effective removal of copper and lower removal of Cd(II) could be attributed to precipitate metal hydroxide formation. For WPE/PAMK-TFN membranes in pressure range 30–50 bar, the relationship between permeate flux and metal rejection of Cd, Cu, and Pb is shown in Figure 11.

It is important to note that lead has provided the highest flux. The rejection decreased with the permeate flux for copper. An almost linear association was found to link the flux of permeates to the rejection of Cu(II). On the contrary, the rejection was found to grow for Cd(II) as the permeate flux increased. For both cadmium and lead, metal rejections were identical at higher and lower fluxes. This finding implies that various pathways reject certain metals.

(3) Effect of Temperature. We note that the reservation for heavy elements is generally high in low temperatures and decreases to about 20% in most items under study. The flow rate of copper ions decreases with the increasing temperature. Lead and cadmium ions increase with increasing temperature, as shown in Figures 12 and 13. We note that the flow rate of lead and cadmium at high temperatures is approximately equal to the difference in the reservation ratio to the elements during the filtration process. Through studying the effect of temperature, it was noticed that its effect is remarkable in all ions, whether in the flow rate or retention. This may be due to the change in the size of the pores in

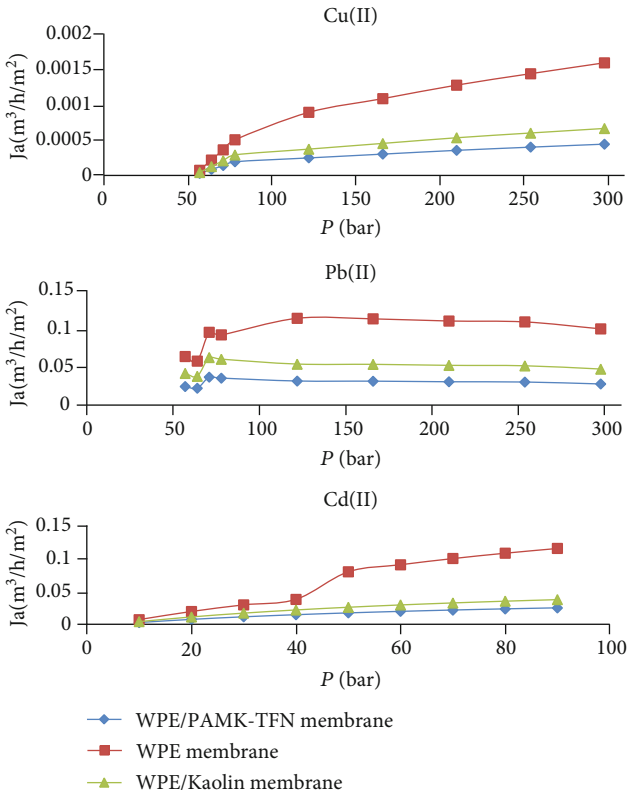

Figure 10: Effect of pressure on the heavy metals filtration on the flow rate of WPS, WPS/kaolin, and WPE/PAMK-TFN membrane.

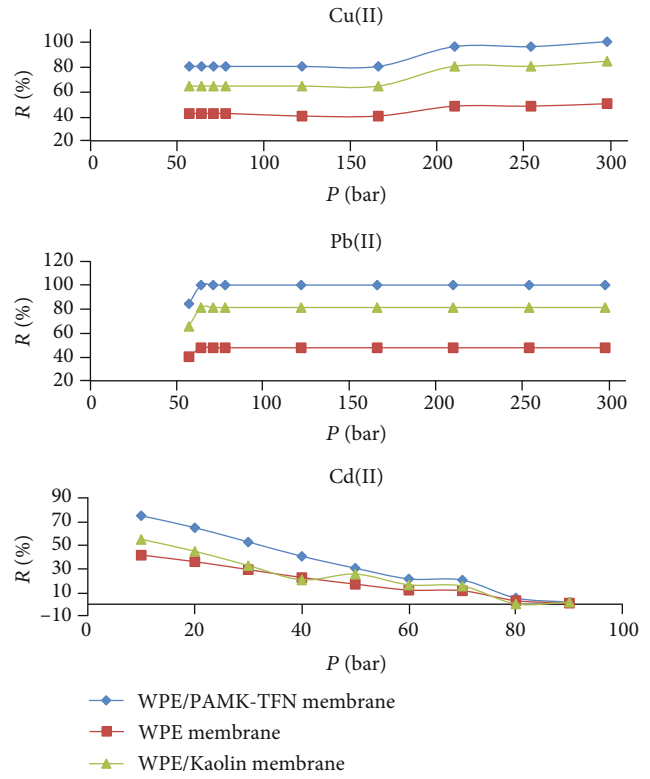

Figure 11: Effect of pressure on rejection of the heavy metals filtration on the WPS, WPS/kaolin, and WPE/PAMK-TFN membranes.

the membrane during the filtering process and the temperature change, which gives an impression of the membrane behavior during the application process in different fields in polluted water temperatures.

(4) Effect of Feed pH Value. Figures 14 and 15 show the removal of Cd, Cu, and Pb with specific anion solutions as a function of the feed pH for 1000 mg/L.

For all studied cations tested, it can be shown that Cd, Cu, and Pb ions are strongly rejected by WPE/PAMK-TFN membranes more than the other two membranes. The disparity in rejection of Cd, Cu, and Pb ions as a function of pH is smaller for divalent cations than that obtained for monovalent cations. That was also observed in other studies involving specific NF membranes. The maximum rejection of Cd, Cu, and Pb ions was observed when the pH value was equal to or slightly higher than the solution's normal pH.

As shown in Figure 15, the removal of Cd, Cu, and Pb ions has a maximum value at pH 11 in WPS/kaolin and WPE/PAMK-TFN membranes. For example, Cd, Cu, and Pb ion rejections were 82, 61, and 44 percent, respectively, for Cd, Cu, and Pb solutions. As the pH of solutions exceeded 4.0 and 3.0, the proton and related anions concentration increased, and the system behaved as a ternary solution (Cd, Cu and Pb, H^+, and anion).

By introducing acids and increasing the concentration of a particular anion between salt and acid, anion's enhanced concentration contributes to an improved and faster passage of cations across the membrane [42]. Due to the relatively reduced size, additional protons are spread through the membrane to preserve the electro-neutrality condition. The Cd, Cu, and Pb ions have been firmly refused due to their higher valence. Naim and Monir [43] indicated that protons at higher acidity could neutralize the membrane surface's harmful sites, especially in WPS/kaolin and WPE/PAMK-TFN membranes, which can reduce the repulsion between the anions and the membrane surface. The rejection of Cd, Cu, and Pb ion increased at pH values higher than the normal pH of the solutions, while the Na^+ concentration and the negative membrane charge showed an increase as well. At higher pH values, the pore membrane size of WPS/kaolin and WPE/PAMK-TFN membranes is smaller owing to the dissociation of carboxyl membrane groups and the repulsion between them, which contributes to higher solute rejection than in the case of WPS membrane.

(5) Rejection and Flux Mechanism as a Function of pH Value. At pH 7.0, insoluble hydroxides' formation comes from metal ions' ability to form complexes with OH^- ions. Membranes readily and ultimately reject these hydroxides; there would be a more significant rejection of lead ions. On the other hand, WPE/PAMK-TFN membranes possess both carboxyl groups OH^- where both at low and high pH values, hydroxyl groupings are, respectively, protonated and deprotonated. For both cases, electrostatic repulsion among the charged groups leads to an increased refusal of the solutes

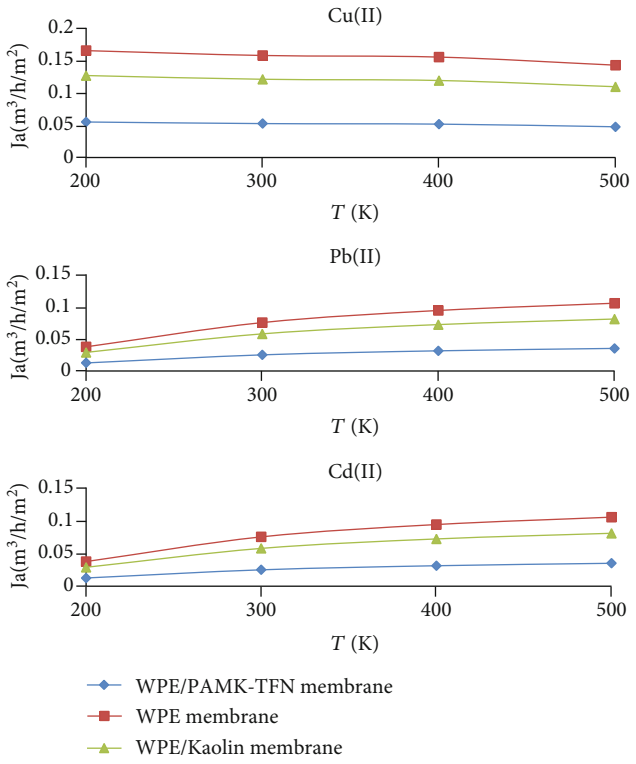

Figure 12: Effect of temperature on the flux of heavy metals on the prepared WPS, WPS/kaolin, and WPE/PAMK-TFN membranes.

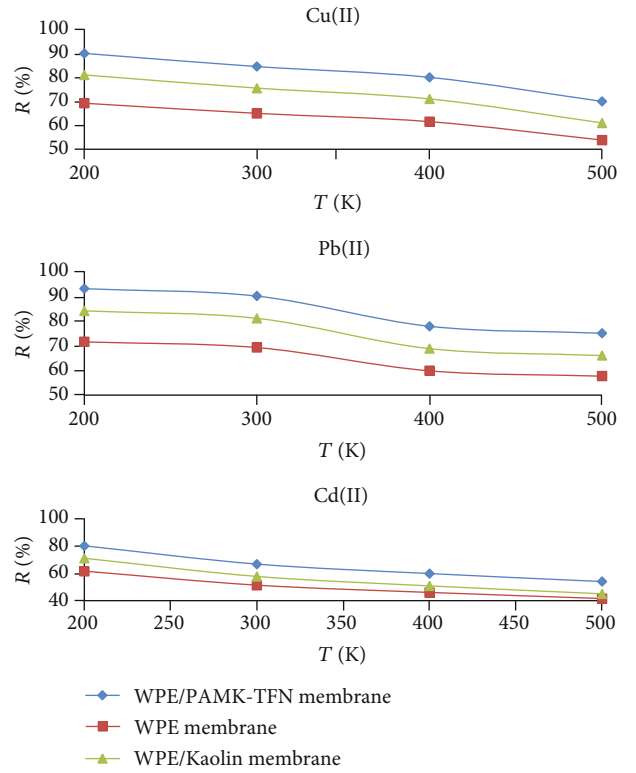

Figure 13: Effect of temperature on the rejection of heavy metals on the prepared WPS, WPS/kaolin, and WPE/PAMK-TFN membranes.

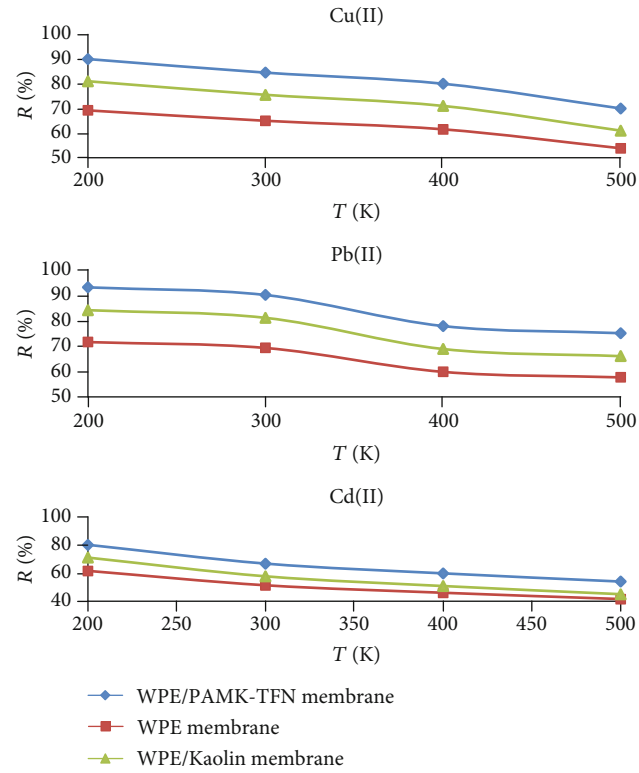

Figure 14: Effect of pH value on the flux of heavy metals on the prepared WPS, WPS/kaolin, and WPE/PAMK-TFN membranes.

involved. The flux permeates over the pH of the feed solution. The permeate flux increased toward pH to a maximum value that reached each solution's normal pH. This can be due to the presence of a membrane isoelectric point at the normal pH of [43, 44]. Childress and Elimelech [45] revealed that this result relates to three factors, namely, membrane pore size, electro-viscous effect, and osmotic pressure gradient of the membrane. Due to these findings, when a charge (positive or negative) is present on the membrane surface, the membrane pore size is smaller. Due to the repulsion on the membrane's active layer between the charged groups and the solutes, it results in less flux and higher rejection. The rejection of the solute was at the highest level at pH 3.0, and the osmotic pressure at the surface of the membrane was more tremendous. Higher osmotic pressure induces a reduction in the net driving pressure leading to a reduction in the permeate flux [46].

(6) Impact of Concentration of Metal Ions. Material recyclability is one of the essential parameters for adsorbent application in the industry. A study on material recyclability was conducted by reuse the regenerated used WPE/PAMK-TFN membrane for 7 cycles. With the initial concentration of metal ions (1000 mg/L), we found that the metal removal efficiency values for Cu(II), Pb(II), and Cd(II) ions were 97.6, 99.1, and 99.5% at pH 5.5-7, respectively. Leaching is using 1 M HCl. The used adsorbent was soaked in the HCl solution for 12 h followed by filtration, washing by double-distilled water, and drying conducted the regeneration of

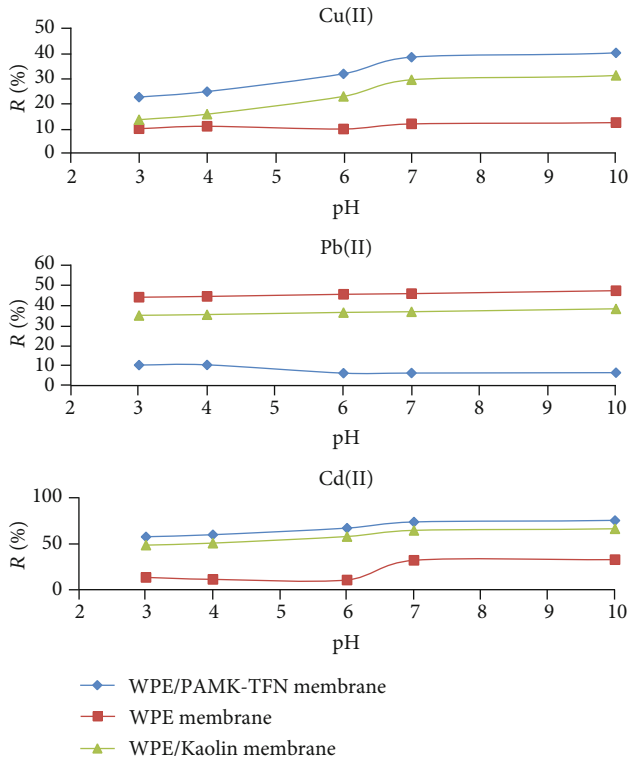

Figure 15: Effect of pH value on the rejection of heavy metals on the prepared WPS, WPS/kaolin, and WPE/PAMK-TFN membranes.

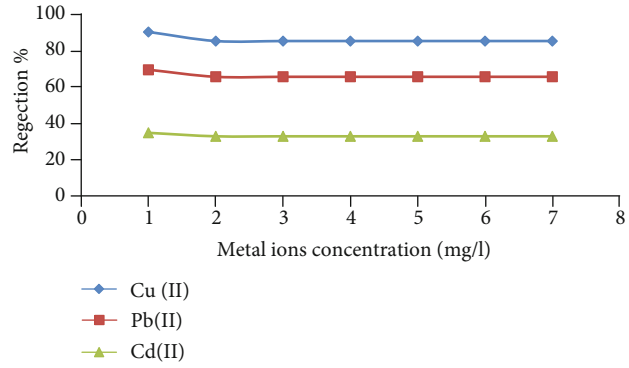

Figure 16: Influence of the WPE/PAMK-TFN membrane filtration cycles on heavy metal ions rejection. (pH 7, $p = 20$ bar).

WPE/PAMK-TFN membrane. For both Pb (II) and Cd (II) ions, the membrane had been effectively controlled at a broad range of concentrations up to 100 mg/L, as shown in Figure 16. However, with Cu(II) ions, the metal removal decreased gradually with a rise in Cu(II) ion concentration; with Cu(II) ion concentration of 200 mg/L, the metal rejection efficiency reduced to 80 percent. It is due to the WPE/-PAMK-TFN membranes having an exceptionally high affinity to certain cations. The cations were graded as Cu(II) > Pb(II) > Cd(II) [47], according to the Irving–Williams series [44], which ranks the divalent metal ions, regardless of the complexing agent type, in their tendency to complexity. The current findings accepted this action for the divalent cations and affirmed that. The metal removal order is found to be Cd(II) > Cu(II) > Pb(II) ions are partly bound to the surface of the WPE/PAMK membranes at a high concentration of metal ions, and, thus, the efficiency of rejection decreases. The rejection of heavy metals (%) using recycled WPE/PAMK-TFN membrane presented in Figure 16 suggests that the material has stable adsorbent capability until seven cycles.

4. Conclusions

In this work, a complexation/ultrafiltration approach for effective removal of heavy metal cations such as Cu(II), Pb(II), and Cd(II) ions from synthetic wastewater solutions has been successfully developed via the construction of novel WPE/PAMK-TFN hybrid material. Results revealed that combined complexation/ultrafiltration processes are pH-dependent, with the metal removal process being more efficient in both neutral and alkaline environments rather than acidic ones. Thus, at pH 7, the metal removal percent efficiency values were estimated and found to be 91.6% and 84.6% for initial metal ion concentration of 550 mg/of Pb(II) and Cd(II) ions, respectively. Notably, the membrane operated highly efficiently over a wide concentration range of up to 600 mg/L for both Cu(II) and Pb(II) ions. In contrast, the removal efficiency of Cd(II) ions decreased to 60%. The constructed WPE/PAMK-TFN membrane showed a higher complexing affinity for Cu(II) than Pb(II) and Cd(II). Finally, the developed method is superior to other methods in terms of low energy requirements for ultrafiltration, swift reaction kinetics, and high selectivity to separate metal ions. Simultaneous isolation of the three metal ions in one boot confirmed the membrane selectivity.

Data Availability

The data used to support the findings of this study are available from the corresponding author upon request.

Conflicts of Interest

The authors declare that they have no conflicts of interest.

Acknowledgments

We extend our sincere appreciation to the Researchers Supporting Project (RSP-2021/79) at King Saud University, Riyadh, Saudi Arabia.

References

[1] U. P. M. Ashik, W. M. A. Wan Daud, and H. F. Abbas, "Production of greenhouse gas free hydrogen by thermocatalytic decomposition of methane – a review," *Renewable and Sustainable Energy Reviews*, vol. 44, pp. 221–256, 2015.

[2] C. Augeray, M. Magalie, B. Nathalie et al., "Development of a protocol to measure iron-55 in solid matrices in the environment," *Journal of Environmental Radioactivity*, vol. 141, pp. 164–173, 2015.

[3] M. Asghari, A. Harandizadeh, M. Dehghani, and H. R. Harami, "Persian gulf desalination using air gap membrane

distillation: numerical simulation and theoretical study," *Desalination*, vol. 374, pp. 92–100, 2015.

[4] A. Matin, H. Z. Shafi, Z. Khan et al., "Surface modification of seawater desalination reverse osmosis membranes: characterization studies & performance evaluation," *Desalination*, vol. 343, pp. 128–139, 2014.

[5] A. Sweity, Z. Ronen, and M. Herzberg, "Induced organic fouling with antiscalants in seawater desalination," *Desalination*, vol. 352, pp. 158–165, 2014.

[6] S. Ali, J. Bae, C. H. Lee, K. H. Choi, and Y. H. Doh, "All-printed and highly stable organic resistive switching device based on graphene quantum dots and polyvinylpyrrolidone composite," *Organic Electronics*, vol. 25, pp. 225–231, 2015.

[7] S. A. Ali, I. W. Kazi, and F. Rahman, "Synthesis and evaluation of phosphate-free antiscalants to control $CaSO_4$ $2H_2O$ scale formation in reverse osmosis desalination plants," *Desalination*, vol. 357, pp. 36–44, 2015.

[8] P. Menoud, L. Cavin, and A. Renken, "Modelling of heavy metals adsorption to a chelating resin in a fluidized bed reactor," *Chemical Engineering and Processing: Process Intensification*, vol. 37, no. 1, pp. 89–101, 1998.

[9] A. Farsi, C. Malvache, O. De Bartolis et al., "Design and fabrication of silica-based nanofiltration membranes for water desalination and detoxification," *Microporous and Mesoporous Materials*, vol. 237, pp. 117–126, 2017.

[10] M. A. Barakat, "New trends in removing heavy metals from industrial wastewater," *Arabian Journal of Chemistry*, vol. 4, no. 4, pp. 361–377, 2011.

[11] M. Ghalamchi, A. Kasaeian, M. Ghalamchi, N. Fadaei, and R. Daneshazarian, "Optimizing of solar chimney performance using electrohydrodynamic system based on array geometry," *Energy Conversion and Management*, vol. 135, pp. 261–269, 2017.

[12] S. Sperinck, P. Raiteri, N. Marks, and K. Wright, "Dehydroxylation of kaolinite to metakaolin—a molecular dynamics study," *Journal of Materials Chemistry*, vol. 21, no. 7, pp. 2118–2125, 2011.

[13] N. A. Oladoja, Y. Liu, J. E. Drewes, and B. Helmreich, "Preparation and characterization of a reactive filter for groundwater defluoridation," *Chemical Engineering Journal*, vol. 283, pp. 1154–1167, 2016.

[14] Y. Niu and M. Xu, "Reduced graphene oxide and Fe2(MoO4)3 composite for sodium-ion batteries cathode with improved performance," *Journal of Alloys and Compounds*, vol. 674, pp. 392–398, 2016.

[15] J. Prince, G. Singh, D. Rana, T. Matsuura, V. Anbharasi, and T. S. Shanmugasundaram, "Preparation and characterization of highly hydrophobic poly(vinylidene fluoride) - Clay nanocomposite nanofiber membranes (PVDF-clay NNMs) for desalination using direct contact membrane distillation," *Journal of Membrane Science*, vol. 397-398, pp. 80–86, 2012.

[16] S. Nandini, S. Nalini, M. B. M. Reddy et al., "Synthesis of one-dimensional gold nanostructures and the electrochemical application of the nanohybrid containing functionalized graphene oxide for cholesterol biosensing," *Bioelectrochemistry*, vol. 110, pp. 79–90, 2016.

[17] G. Mustafa, P. P. Nandekar, T. J. Camp et al., "Influence of transmembrane helix mutations on cytochrome P450-membrane interactions and function," *Biophysical Journal*, vol. 116, no. 3, pp. 419–432, 2019.

[18] H. Pichler and A. Emmerstorfer-Augustin, "Modification of membrane lipid compositions in single-celled organisms – from basics to applications," *Methods*, vol. 147, pp. 50–65, 2018.

[19] M. Arshadi, S. Foroughifard, J. Etemad Gholtash, and A. Abbaspourrad, "Preparation of iron nanoparticles-loaded *Spondias purpurea* seed waste as an excellent adsorbent for removal of phosphate from synthetic and natural waters," *Journal of Colloid and Interface Science*, vol. 452, pp. 69–77, 2015.

[20] S. Araby, N. Saber, X. Ma et al., "Implication of multi-walled carbon nanotubes on polymer/graphene composites," *Materials & Design*, vol. 65, pp. 690–699, 2015.

[21] B. A. M. Al-Rashdi, D. J. Johnson, and N. Hilal, "Removal of heavy metal ions by nanofiltration," *Desalination*, vol. 315, pp. 2–17, 2013.

[22] H. B. Bacha, W. Masmoudi, A. Y. Maalej, and H. B. Dhia, "Software for sizing and simulating of SMCEC desalination process," *Desalination*, vol. 165, pp. 421–433, 2004.

[23] B. Zhu, X. Hu, J.-W. Shin et al., "A method for defect repair of MFI-type zeolite membranes by multivalent ion infiltration," *Microporous and Mesoporous Materials*, vol. 237, pp. 140–150, 2017.

[24] Z. Zhang and D. Huisingh, "Carbon dioxide storage schemes: technology, assessment and deployment," *journal of cleaner production*, vol. 142, pp. 1055–1064, 2017.

[25] J. Zheng, M. Li, K. Yu, J. Hu, X. Zhang, and L. Wang, "Sulfonated multiwall carbon nanotubes assisted thin-film nanocomposite membrane with enhanced water flux and anti-fouling property," *Journal of Membrane Science*, vol. 524, pp. 344–353, 2017.

[26] S. Hao, Z. Jia, J. Wen et al., "Progress in adsorptive membranes for separation – a review," *Separation and Purification Technology*, vol. 255, article 117772, 2021.

[27] T. Luukkonen, H. Runtti, M. Niskanen et al., "Simultaneous removal of Ni(II), As(III), and Sb(III) from spiked mine effluent with metakaolin and blast-furnace-slag geopolymers," *Journal of Environmental Management*, vol. 166, pp. 579–588, 2016.

[28] M. Fathy, T. Abdel Moghny, M. A. Mousa, A.-H. A.-A. El-Bellihi, and A. E. Awadallah, "Absorption of calcium ions on oxidized graphene sheets and study its dynamic behavior by kinetic and isothermal models," *Applied Nanoscience*, vol. 6, no. 8, pp. 1105–1117, 2016.

[29] M. el-Sayed, M. Ramzi, R. Hosny, M. Fathy, and T. Abdel Moghny, "Breakthrough curves of oil adsorption on novel amorphous carbon thin film," *Water Science and Technology*, vol. 73, no. 10, pp. 2361–2369, 2016.

[30] E. Song, K. Wei, H. Lian et al., "Improved propylene/propane separation performance under high temperature and pressures on in-situ ligand-doped ZIF-8 membranes," *Journal of Membrane Science*, vol. 617, article 118655, 2021.

[31] L. Huang, R. Liu, J. Yang et al., "Nanoarchitectured porous organic polymers and their environmental applications for removal of toxic metal ions," *Chemical Engineering Journal*, vol. 408, article 127991, 2021.

[32] C. Y. Chuah, Y. Lee, and T.-H. Bae, "Potential of adsorbents and membranes for SF6 capture and recovery: a review," *Chemical Engineering Journal*, vol. 404, article 126577, 2021.

[33] M. E. Awad, A. López-Galindo, M. Setti, M. M. El-Rahmany, and C. V. Iborra, "Kaolinite in pharmaceutics and biomedicine," *International Journal of Pharmaceutics*, vol. 533, no. 1, pp. 34–48, 2017.

[34] H. Tu, M. Huang, Y. Yi et al., "Chitosan-rectorite nanospheres immobilized on polystyrene fibrous mats via alternate electrospinning/electrospraying techniques for copper ions adsorption," *Applied Surface Science*, vol. 426, pp. 545–553, 2017.

[35] M. Shariful, S. Talebian, M. Mehrali, B. Ang, and M. Amal, "Corrigendum: adsorption capability of heavy metals by chitosan/poly (ethylene oxide)/activated carbon electrospun nanofibrous membrane," *Journal of Applied Polymer Science*, vol. 135, no. 14, article 46083, 2018.

[36] R.-X. Wu, G.-F. Zheng, W.-W. Li, L.-B. Zhong, and Y.-M. Zheng, "Electrospun chitosan nanofiber membrane for adsorption of Cu (II) from aqueous solution: fabrication, characterization and performance," *Journal of Nanoscience and Nanotechnology*, vol. 18, no. 8, pp. 5624–5635, 2018.

[37] W. S. Wan Ngah, C. Endud, and R. Mayanar, "Removal of copper(II) ions from aqueous solution onto chitosan and cross-linked chitosan beads," *Reactive and Functional Polymers*, vol. 50, no. 2, pp. 181–190, 2002.

[38] S. Haider, F. A. A. Ali, A. Haider, W. A. Al-Masry, and Y. Al-Zeghayer, "Novel route for amine grafting to chitosan electrospun nanofibers membrane for the removal of copper and lead ions from aqueous medium," *Carbohydrate Polymers*, vol. 199, pp. 406–414, 2018.

[39] M. M. Rahman, J. Ahmed, A. M. Asiri, I. A. Siddiquey, and M. A. Hasnat, "Development of 4-methoxyphenol chemical sensor based on NiS_2-CNT nanocomposites," *Journal of the Taiwan Institute of Chemical Engineers*, vol. 64, pp. 157–165, 2016.

[40] M. S. Aljohani, "Nuclear desalination competitiveness in the western region of the Kingdom of Saudi Arabia," *Desalination*, vol. 164, no. 3, pp. 213–223, 2004.

[41] L. Tian, Y. Wang, and J. Guo, "A comparative economic analysis of the contribution of nuclear seawater desalination to environmental protection using the clean development mechanism (CDM)," *Desalination*, vol. 157, no. 1-3, pp. 289–296, 2003.

[42] A. G. Pervov, A. P. Andrianov, R. V. Efremov, A. V. Desyatov, and A. E. Baranov, "A new solution for the Caspian Sea desalination: low-pressure membranes," *Desalination*, vol. 157, no. 1-3, pp. 377–384, 2003.

[43] M. M. Naim and A. A. Monir, "Desalination using supported liquid membranes," *Desalination*, vol. 153, no. 1-3, pp. 361–369, 2003.

[44] P. S. Goh, A. F. Ismail, and N. Hilal, "Nano-enabled membranes technology: sustainable and revolutionary solutions for membrane desalination?," *Desalination*, vol. 380, pp. 100–104, 2016.

[45] A. E. Childress and M. Elimelech, "Relating nanofiltration membrane performance to membrane charge (electrokinetic) characteristics," *Environmental Science & Technology*, vol. 34, no. 17, pp. 3710–3716, 2000.

[46] S. Mehdipour, V. Vatanpour, and H.-R. Kariminia, "Influence of ion interaction on lead removal by a polyamide nanofiltration membrane," *Desalination*, vol. 362, pp. 84–92, 2015.

[47] L. García-Cruz, C. Casado-Coterillo, J. Iniesta, V. Montiel, and Á. Irabien, "Chitosan:poly (vinyl) alcohol composite alkaline membrane incorporating organic ionomers and layered silicate materials into a PEM electrochemical reactor," *Journal of Membrane Science*, vol. 498, pp. 395–407, 2016.